Biomaterials 34 (2013) 875–887

Contents lists available at SciVerse ScienceDirect

Biomaterials

journal homepage: www.elsevier.com/locate/biomaterials

Neurite outgrowth and synaptophysin expression of postnatal CNS neurons on GaP nanowire arrays in long-term retinal cell culture

Gaëlle Piret [a,b,c], Maria-Thereza Perez [c,d,**], Christelle N. Prinz [a,b,*]

[a] Division of Solid State Physics, The Nanometer Structure Consortium, Lund University, Sweden
[b] Neuronano Research Center, Lund University, Sweden
[c] Department of Clinical Sciences, Division of Ophthalmology, Lund University, Sweden
[d] Department of Ophthalmology, Glostrup Hospital, Glostrup, Denmark

ARTICLE INFO

Article history:
Received 30 September 2012
Accepted 16 October 2012
Available online 3 November 2012

Keywords:
Nanowires
Nanotopography
CNS
Retina
Neuron
Glia

ABSTRACT

We have established long-term cultures of postnatal retinal cells on arrays of gallium phosphide nanowires of different geometries. Rod and cone photoreceptors, ganglion cells and bipolar cells survived on the substrates for at least 18 days *in vitro*. Glial cells were also observed, but these did not overgrow the neuronal population. On nanowires, neurons extended numerous long and branched neurites that expressed the synaptic vesicle marker synaptophysin. The longest nanowires (4 μm long) allowed a greater attachment and neurite elongation and our analysis suggests that the length of the nanowire *per se* and/or the adsorption of biomolecules on the nanowires may have been important factors regulating the observed cell behavior. The study thus shows that CNS neurons are amenable to gallium phosphide nanowires, probably as they create conditions that more closely resemble those encountered in the *in vivo* environment. These findings suggest that gallium phosphide nanowires may be considered as a material of interest when improving existing or designing the next generation of implantable devices. The features of gallium phosphide nanowires can be precisely controlled, making them suitable for this purpose.

1. Introduction

Substrate chemistry and topography are among the factors that influence cell viability and behavior, both *in vivo* and *in vitro* [1,2]. These parameters can be easily tuned in engineered materials and both micro and nanofabricated surfaces have been used for neural interfaces, for stem cell differentiation, or for drug delivery [1–8]. The development of fabrication methods is therefore expected to play an important role in the improvement of *in vitro* and *in vivo* protocols. Brain implants, for instance, are used for tempering the symptoms of Parkinson's disease or help locked-in patients to communicate [9]. They usually consist of electrodes with a smooth surface, which elicits a tissue response, leading to the formation of an isolating layer around the electrodes and to decreased signal levels [10]. It has recently been shown that nanostructured surfaces result in lower tissue response to the implant and improved recording properties of the electrodes [3,11].

Nanowires are one-dimensional objects, with a diameter in the nanometer range and a length on the micrometer length scale. Several studies have explored possible nanowire applications in biology and investigated the biocompatibility of nanowire suspensions and nanowire arrays [8,12–19]. In these studies, nanowires were composed of a single material (silicon, gallium arsenide, gallium phosphide or metal) and in the case of arrays, these had a fixed topography (diameter, length, pitch). One recent study has investigated the effect of topography in silicon-nanopillar-arrays on stem cell fate [20]. However, the influence of specific topographical parameters on biocompatibility and functionality remains ill-defined.

Nanowire arrays of gallium phosphide (GaP), a III–V semiconductor material, can be produced by using metal organic vapor-phase epitaxy [21]. The resulting nanowires (GaP NW) stand perfectly vertical on the substrate, are monodisperse in size and their specific geometry can be easily controlled [12,17,22]. We have previously shown that GaP NW substrates support and guide the growth of peripheral nervous system neurons, with cell focal adhesions forming on the nanowires [12,14,15]. Here, we

* Corresponding author. Division of Solid State Physics, The Nanometer Structure Consortium, Lund University, SE-221 00 Lund, Sweden. Tel.: +46 462224796.
** Corresponding author. Department of Clinical Sciences, Division of Ophthalmology, Lund University, SE-221 84 Lund, Sweden. Tel.: +46 462220772.
E-mail addresses: maria_thereza.perez@med.lu.se (M.-T. Perez), christelle.prinz@ftf.lth.se (C.N. Prinz).

0142-9612
http://dx.doi.org/10.1016/j.biomaterials.2012.10.042

have performed an initial characterization of the survival and behavior of central nervous system (CNS) cells cultured on these substrates.

Retinal cells derived from early postnatal mice were used in the study. The retina, being a part of the CNS, is susceptible to degenerative processes, but is also amenable to many of the treatment possibilities explored for brain diseases, such as neuroprotection and cell replacement. However, as others and we have shown, physical and molecular barriers exist in a degenerating retina that limit the successful outcome of these treatments [23–25]. More recently, nanotechnology applications have been directed also towards retinal diseases, including the development of nanoparticles capable of delivering genes and neuroprotective molecules (reviewed in Ref. [26]) as well as the fabrication of scaffolds with nanoscale topographies for the intraocular delivery of cells [27]. Another treatment modality being tested to treat retinal degenerations involves the use of sub or epiretinal implants [26,28,29], a field where nanocomponents have a great potential, in particular those that allow a good control of their surface topography.

In the present study, we exploited the fact that various parameters of GaP NW array topography can be tuned and adjusted independently, and used these arrays as a model system to test whether they may be suitable for implants.

2. Materials and methods

2.1. Animals

Wild-type mice (C3H/HeA background, own colonies) were kept on a 12-h light–dark cycle, with free access to food and water. All experiments were approved by the local committee for animal experimentation and ethics. Handling of animals was in accordance with the ARVO Statement for the Use of Animals in Ophthalmic and Vision Research.

2.2. Nanowire substrate preparation

The GaP NW were grown by metal organic vapor-phase epitaxy (MOVPE) from Au catalytical seeds [21]. Au nanoparticles were deposited on a GaP (111)B substrate using a dedicated aerosol set-up [30]. The substrates were thereafter transferred to a growth chamber (Aix 200/4, Aixtron AG, Germany) and nanowire growth was carried out at 470 °C. The wire growth was initiated by supplying $Ga(CH_3)_3$ in addition to PH_3, with respective precursor molar fractions of $4.3 \cdot 10^{-6}$ and $8.5 \cdot 10^{-2}$ in hydrogen carrier gas flow of 6 L/min, and under a pressure of 10 kPa. Under those conditions, the wire length is controlled by the growth time and the nanowire diameter by the gold nanoparticle size. The resulting wires grow in the [111]B direction (vertical on the surface).

In order to examine the effect of different substrate topographies on cell behavior, arrays were produced with distinct geometries (see Table 1). Each substrate (with an area of about 10 mm^2) was composed of identical wires of a specific length (0.5, 1 or 4 μm), diameter (20, 40 or 80 nm) and density (0.2, 1, 2, 3 or 10 NW/μm^2). Some of these different GaP NW substrates are shown in Fig. 1. In a few cases, substrates were coated with hafnium oxide (HfO_x) by atomic layer deposition (ALD) using a Savannah-100 system (Cambridge NanoTech Inc., USA) in order to deposit a homogeneous layer of 20 nm of oxide. Control substrates consisted of flat GaP of the same size as the GaP NW substrates. Before cell seeding, substrates were incubated in 70% ethanol for 10 min, air-dried overnight and placed in sterile 4-well culture chambers (Nunc Lab-Tek II Chamber Slide System, Thermo Scientific, Denmark; code: 177399).

2.3. Primary retinal cell culture

Retinal cultures were prepared as previously described in Ref. [31] with only a few modifications. Briefly, a digestion solution was prepared with papain (18 Units/mL, Worthington Biochemical Corp, USA; code LS003118) at 1 mg/mL and L-cysteine (Sigma–Aldrich Sweden AB, Sweden; code C7477) at 0.3 μg/mL in Dulbecco's modified Eagle's Medium (DMEM) (Invitrogen Life Technologies, Sweden; code 41966-029). The digestion solution was incubated at 37 °C during 10 min, filtered with a 0.22 μm pore filter (SARSTEDT, Germany; code 83-1826-001) and used within 1 h. Retinas were isolated from postnatal (PN) day 4 mice under R16 serum-free culture medium (Invitrogen Life Technologies, UK; code 07490743A) [32] free from retinal pigment epithelium and transferred thereafter to a digestion solution (0.75 mL/retina) for 30 min at 37 °C. The retinal tissue was then carefully rinsed with 3 × 10 mL DMEM. Subsequently, 2 mL of culture medium [DMEM containing 2% of B27-supplement (Invitrogen Life Technologies, Sweden; code 17504-044) and 2% of L-glutamine–penicillin–streptomycin solution (Sigma–Aldrich Sweden AB, Sweden; code G6784)] were added to the retinal tissue, which was dissociated using a Pasteur pipette. The suspension was then transferred to a new vial containing 48 mL of DMEM at 37 °C and spun down for 5 min at 900× *g* at room temperature. The supernatant was removed and the cell pellet was resuspended in the culture medium solution (2.27 mL/retina). The retinal cell suspension was passed through a cell strainer with a 40 μm nylon mesh (BD Biosciences, USA; code 352340) and 500 μL (approximately 9×10^4 cells) were seeded onto each well, each one containing one type of GaP NW or flat GaP substrate. Twenty-two culture experiments were performed on different days with an average of 12 substrates per experiment.

Table 1
Nanowire substrates used in the study.

Diameter (nm)	Length (μm)	Density (NW/μm^2)	Chemistry
40/80	4	1	GaP
20/40/80	1	1	GaP
80	0.5	1/10	GaP
80	4	0.2/1/2/3/10	GaP
80	4	1	HfO_x

2.4. TUNEL assay

After culturing for 3, 6, 12, and 18 days *in vitro* (DIV), 4% paraformaldehyde (PFA) in 100 mM Sørensen's buffer (pH = 7.4) was added to the culture medium for 10 min. After removing the solution, fresh PFA was applied for 30 min, followed by 3× 10 min with PBS (10 mM, pH = 7.2). Dying cells were detected with a terminal deoxynucleotidyl transferase dUTP nick end labeling (TUNEL) assay, employing the *In Situ* Cell Death Detection Kit, TMR red (Roche Diagnostics, Germany; code 12156792910), as previously described in Ref. [33]. The enzyme solution was diluted 1:9 and the labeling solution 1:4 in PBS. The two components were mixed 1:4.44 immediately before application to the cells for 1 h at 37 °C in the dark. The reaction was stopped by 3 washes with cold PBS. The substrates containing the cells were mounted with the anti-fading medium VECTASHIELD containing the nucleic acid stain 4′,6-diamidino-2-phenylindole (DAPI) (Vector Laboratories, USA; code H-1200).

2.5. Immunocytochemistry

Following 3DIV and 18DIV, the cultured cells were fixed and rinsed (as above) and then blocked and permeabilized by pre-incubation for 30 min at room temperature with Tris-buffered saline (TBS; 10 mM, pH 7.2) containing 0.25% Triton X-100 (TBS-T) and 2% bovine serum albumin (BSA). Cells were subsequently incubated overnight at 4 °C with TBS-T containing the monoclonal or polyclonal primary antibodies listed in Table 2, followed by 3× 10 min washes with TBS. Samples were then incubated with secondary antibodies: DyLight-488 donkey anti-rabbit (Jackson ImmunoResearch Laboratories Inc., USA; code 711-485-152), DyLight-549 donkey anti-mouse (Jackson ImmunoResearch Laboratories Inc., USA; code 715-505-150), Alexa-488 donkey anti-goat (Invitrogen Life Technologies, Sweden; code A11055) or Texas Red donkey anti-sheep (Jackson ImmunoResearch Laboratories Inc., USA; code 713-076-147) at 1:200 for 90 min at room temperature. For retinal sections, animals were sacrificed at PN7 and PN22. Eyes were enucleated and fixed in 4% paraformaldehyde (PFA) in 100 mM Sørensen's buffer (pH = 7.4) for 2 h at 4 °C. The tissue was subsequently rinsed and cryoprotected by increasing concentrations of sucrose in the buffer. The eyes were embedded in an albumin–gelatin medium and frozen. Twelve-micrometer cryostat sections were collected on gelatin/chrome alum-coated glass slides and air-dried before storage at −20 °C. Cryosections were blocked and permeabilized by pre-incubation for 45 min at room temperature with PBS containing 0.25% Triton X-100, 1% bovine serum albumin (BSA) and 5% normal serum (PBS-TS). The sections were thereafter incubated overnight at 4 °C with the antibodies listed in Table 2 dissolved in PBS-T containing normal serum, followed by a 45 min incubation with the corresponding secondary antibodies (listed above). Cell and retinal samples were rinsed 3× 10 min with PBS and mounted with VECTASHIELD containing DAPI.

2.6. Fluorescence microscopy

Retinal cultures and sections were examined with a wide field fluorescence microscope (Axiophot, Carl Zeiss Meditec Inc., Germany) using a plan-neofluar objective (40×/0.75) and a confocal microscope (Zeiss LSM 510, Germany). The confocal images were acquired using a 20×/0.5 air objective with an optical slice of 43 μm or a 40×/0.5 oil immersion objective with an optical slice of either 11.1 μm or 1 μm (corresponding to 1 airy unit).

2.7. Scanning electron microscopy

Cells were fixed by replacing the culture medium with sodium cacodylate buffer (100 mM, pH = 7.4) containing 2.5% of glutaraldehyde. After 30 min, the substrates were rinsed 2× 10 min with fresh buffer and 1× 10 min with ultrapure water

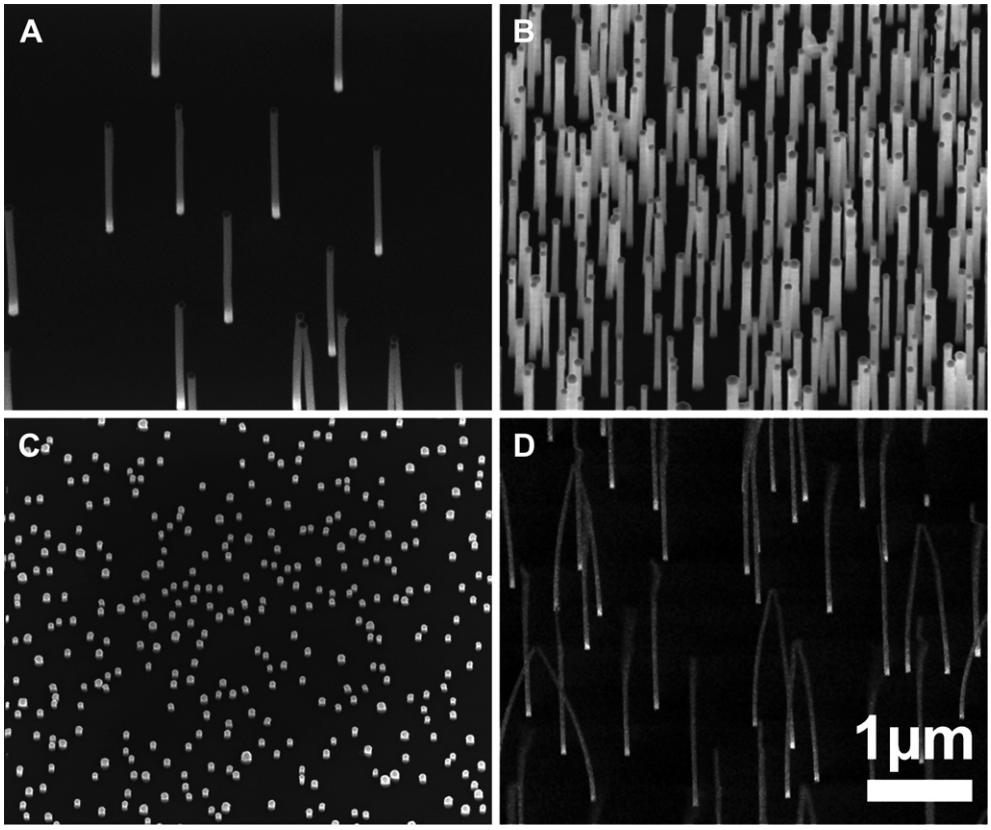

Fig. 1. SEM images showing different GaP NW substrate topographies with (A) a density of 1 NW/μm^2, a diameter of 80 nm and a length of 4 μm, (B) a density of 10 NW/μm^2, a diameter of 80 nm and a length of 4 μm, (C) a density of 10 NW/μm^2, a diameter of 80 nm, and a length of 300 nm, (D) a density of 2 NW/μm^2, a diameter of 40 nm and a length of 4 μm. The collapse of 40 nm diameter NW is due to charging effects during SEM imaging. Tilt 30°. Scale bar, 1 μm for all panels.

(resistivity of 18.2 MΩ cm). The substrates were then dehydrated in a series of ethanol solutions and dried using a critical-point dryer (CPD030, Leica Microsystems GmbH, Wetzlar, Germany). Thereafter, they were sputter-coated with 10 nm of gold-palladium (VG Microtech, SC7640). The scanning electron microscopy study was performed using a LEO SEM 1560, Zeiss (Germany).

3. Results

Several neuronal cell types and glial cells are present in retinas derived from PN4 mice. In order to identify the different

Table 2
Primary antibodies used in the analyses.

Antibody–antigen	Type; host	Dilution: cultures (sections)	Source; code	Retinal distribution [Reference]
β-tubulin, isotype III	MAb; Mouse	1:1500 (1:1500)	Sigma–Aldrich Sweden AB, Sweden; T8660	Inner retinal neurons [48]
Ki67	MAb; Mouse	1:50 (1:50)	Novocastra Laboratories, UK; NCL-Ki67-MM1	Proliferating cells [54]
Synaptophysin	MAb; Mouse	1:50 (1:50)	DAKO A/S, Denmark; M0776	Plexiform layers [51]
Rho 1D4	MAb; Mouse	1:150 (1:150)	Robert S Molday, Univ of British Columbia, Canada	Rods [55]
Cone arrestin	PAb; Rabbit	1:500 (1:1000)	Cheryl Craft, Univ Southern California, USA	Cones [56]
Recoverin	PAb; Rabbit	1:10,000 (1:12,000)	Chemicon Intl, USA; AB5585	Rods, cones, cone bipolar cells [57]
PKC	MAb; Mouse	1:800 (1:800)	Meridian Life Science Inc, USA; K01107M	Bipolar cells [58]
Chx10	PAb; Sheep	1:300 (1:300)	Exalpha Biologicals, Inc., USA; X1179P	Bipolar cells, progenitor cells [59]
Brn-3a	PAb; Goat	1:50 (1:200)	Santa Cruz Biotechnology, Inc, USA; sc-31984	Retinal ganglion cells [49]
TRPV4	PAb; Rabbit	1:600 (1:800)	LifeSpan BioSciences, Inc, USA; LS-C94498	Retinal ganglion cells [60]
GAFP	PAb; Rabbit	1:700 (1:1500)	DAKO A/S, Denmark; Z0334	Glial cells [52]
CRALBP	PAb; Rabbit	1:5000 (1:5000)	John C Saari, University of Washington, USA	Müller glial cells, retinal pigment epithelium [61]

PKC, protein kinase C; TRPV4, transient receptor potential cation channel, subfamily V, member 4; GFAP, glial fibrillary acidic protein; CRALBP, cellular retinaldehyde binding protein; PAb, polyclonal antibody; MAb, monoclonal antibody.

cell types found in the cultures, these were screened for a variety of specific cell markers. Assuming that the maturation process in cultured cells follows approximately the normal developmental program, cells found at 3DIV and 18DIV would correspond to an age of PN7 and PN22, respectively. Thus, in some of the following figures, an image showing the localization of each cell marker in normal retinas at these ages is also provided for orientation.

To establish the presence of neuronal cells, retinal sections and cultures were stained with an antibody against neuron-specific class III β-tubulin. In sections, both at PN7 and PN22, staining was observed in the cytoplasm of ganglion cells, in processes in the inner plexiform layer, and in the nerve fiber layer (Fig. 2A, Fig. S4A). In cultures, β-tubulin III staining was observed among single cells, in cells belonging to cell clusters and in cell processes (Fig. 2B–G). However, significant differences were observed depending on the substrate topography.

3.1. Effect of the topography of GaP NW substrates

Cells were grown on substrates with different topographies (Table 1) and the length and abundance of β-tubulin III positive processes were used to assess which of the substrate parameters tested was the most important in supporting neurite outgrowth. On flat substrates, only a few labeled processes were seen to extend outside the cell clusters both at 3DIV and 18DIV (Fig. 2B; Fig. S4B) even in areas containing numerous clusters. The same was in fact observed with cells grown on short (0.5 μm long) GaP NW (Fig. 2C). Increasing the NW length to 1 μm, however, was already sufficient to enhance neurite outgrowth, irrespective of the diameter of the NW (Fig. 2D–E). Nevertheless, the most striking difference was noted with 4 μm long NW. Already at 3DIV, a dense network of short and long β-tubulin III stained processes was observed in GaP NW (Fig. S4C), a pattern that was even more evident at 18DIV (Fig. 2F–G). In the latter, labeled processes of

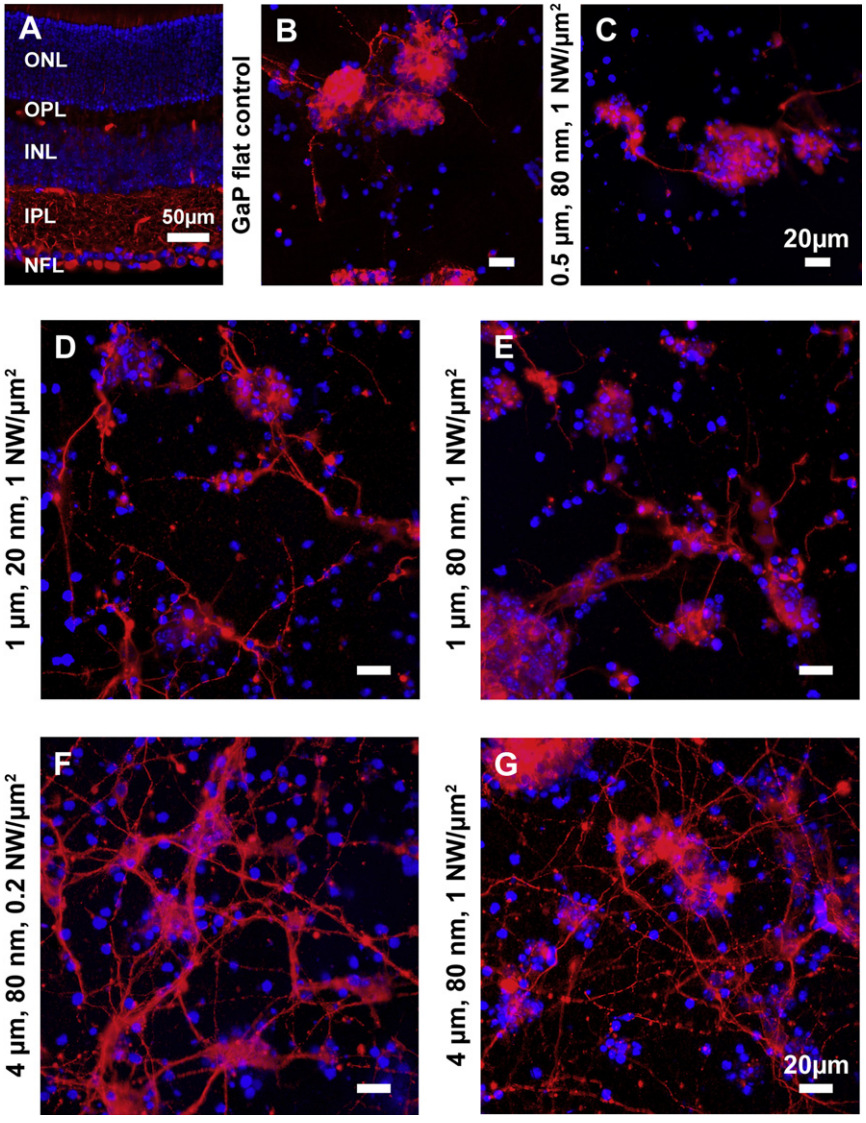

Fig. 2. Fluorescence images showing all cell nuclei (DAPI, blue) and neuronal cells identified by their immunoreactivity for β-tubulin III (red) in (A) a retinal section at PN22, and (B–G) retinal cell cultures after 18DIV on flat GaP and GaP NW substrates with different topographies (specified on the left side of each image). Panels (C), (E) and (G) show that using longer nanowires promoted extensive neuronal outgrowth. On the other hand, changing the NW diameter, as shown in panels (D) and (E), or changing the NW density, as shown in panels (F) and (G) had no major effect on neurite length or their abundance. ONL, outer nuclear layer; OPL, outer plexiform layer; INL, inner nuclear layer; IPL, inner plexiform layer; NFL, nerve fiber layer. Scale bar for retinal section, 50 μm. Scale bars for retinal cell cultures, 20 μm. (For interpretation of the references to color in this figure legend, the reader is referred to the web version of this article.)

different diameters were seen crisscrossing the substrate, seemingly interconnecting several cell clusters. There was an apparent effect of NW density between 0.2 and 1 NW/μm^2 in terms of neurite thickness, but with no obvious effect on the length (Fig. 2F–G). Given that the extent of neurite outgrowth was greatest with the longest NW (4 μm long), the subsequent analyses were all performed using this length. In previous studies, GaP NW with a diameter of 80 nm and a density of 1 NW/μm^2 were used [15,16], and these parameters were also chosen in the present analysis.

3.2. General cell culture characteristics on substrates

We assessed the overall cell distribution at 3DIV and 18DIV by visualizing DAPI-stained nuclei. In a comparison between flat GaP and GaP NW surfaces, it was found that single cells as well as cell aggregates of irregular shape could be observed on both types of substrates. On flat GaP, the cell clusters were of mainly two sizes: large (90–200 μm wide) and medium (50–90 μm wide) (Fig. 3A,C). In addition, relatively few small clusters (less than 50 μm) and numerous single cells were observed. On GaP NW substrates, the number of single cells was generally lower and although large and medium aggregates could occasionally be found, smaller clusters dominated (Fig. 3B,D). It was also evident that the GaP NW substrates were more densely populated with cells (Fig. 3B,D), whereas on flat GaP substrates, areas devoid of cells were noted, particularly at 18DIV (Fig. 3C).

Scanning electron microscopy (SEM) revealed cells of different sizes and morphology (Fig. 4). It confirmed also the presence of multiple processes running mostly between cell clusters, particularly when cells were plated onto GaP NW (Fig. 4B). In order to see whether these interconnecting processes contained the synaptic vesicle protein synaptophysin, cultures were immunostained with an antibody against this protein. In normal mouse retinas, synaptophysin was observed in the plexiform layers at PN7 and PN22 (Fig. 5A, Fig. S4D). Synaptophysin-positive profiles were found in all the cultures and were more often associated with cell clusters. Weakly labeled processes could also be seen running between clusters in GaP NW substrates, but not in flat GaP (Fig. 5B–C, Fig. S4E–F).

Dying cells were detected by TUNEL staining, which revealed a few positive cells, irrespective of the substrate or culture time

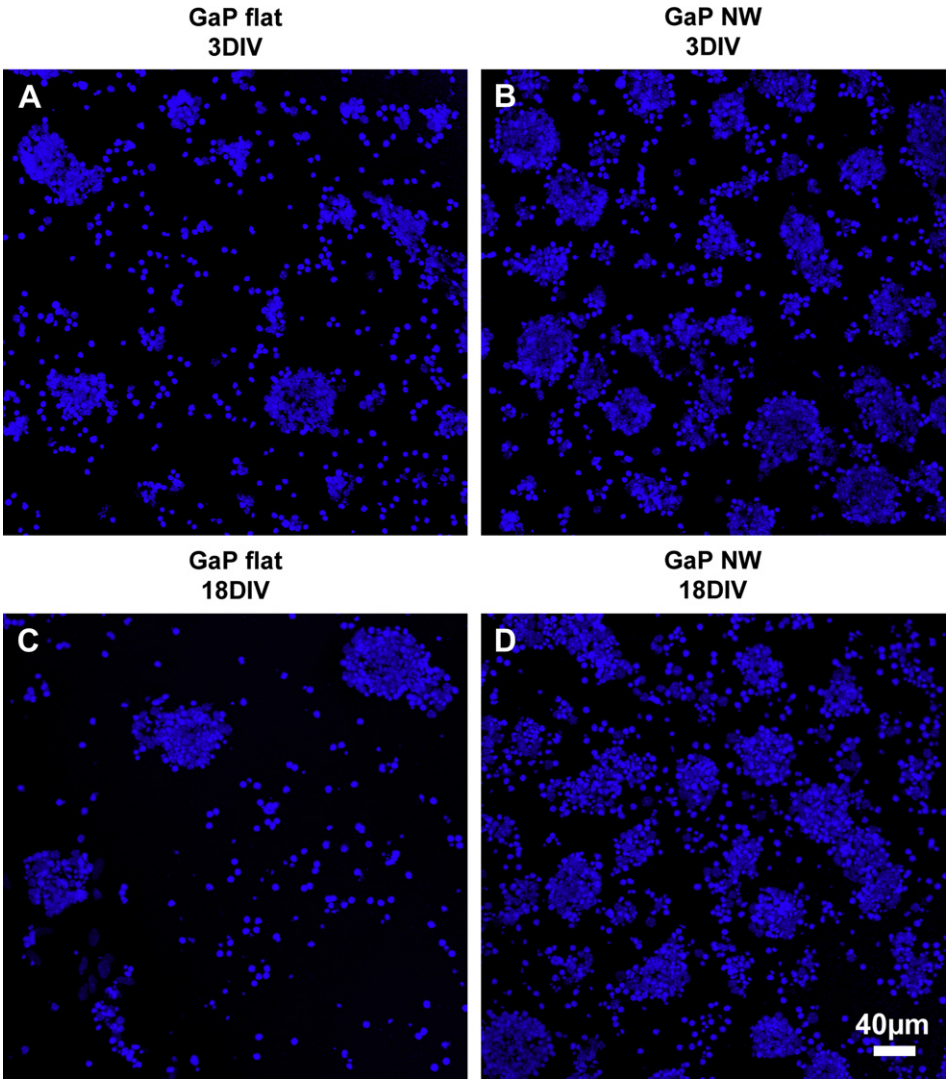

Fig. 3. Fluorescence images of cell nuclei (DAPI) showing the cell distribution on (A) the flat GaP substrate at 3DIV, (B) the GaP NW substrate at 3DIV, (C) the flat GaP substrate at 18DIV, and (D) the GaP NW substrate at 18DIV. In panels (B) and (D), the NW were grown with a density of 1 NW/μm^2, a diameter of 80 nm and a length of 4 μm. Scale bar, 40 μm for all panels.

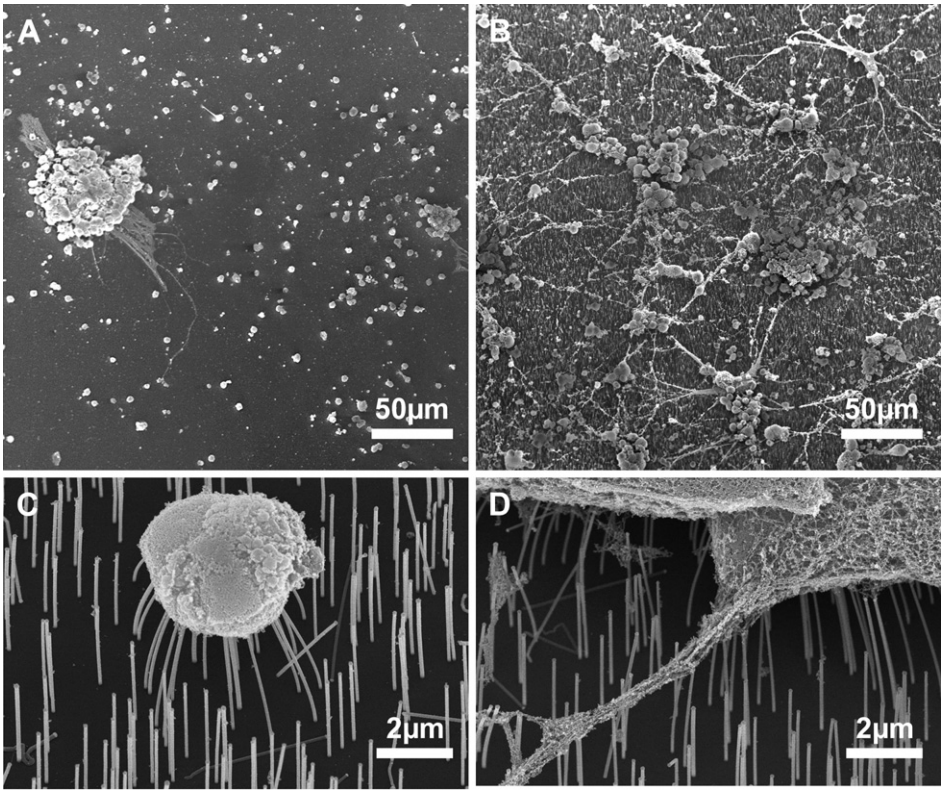

Fig. 4. SEM images of retinal cells cultured on (A) flat GaP and (B–D) on GaP NW substrates. Panels (A) and (B) show retinal cells after 18DIV. Panels (C) and (D) show a close-up of retinal cells after 3DIV. The NW were grown with a density of 1 NW/μm^2, a diameter of 80 nm and a length of 4 μm. Tilt 30°. Scale bar, 50 μm for upper panels and 2 μm for lower panels.

period (Fig. S2). An assessment of cell proliferation by Ki-67 immunostaining showed that a small number of cells expressed the antigen. These were also seen on both types of substrate, with no apparent difference in the overall number of labeled cells between the various samples (Fig. S3). Further, it was noted that both single cells and cells belonging to clusters were among the dying or the proliferating cells, with no obvious correlation.

3.3. Cell diversity

We next examined the ability of the cultured cells to express specific retinal cell markers. Rhodopsin is expressed in normal retinas mostly in the outer segment region of rod photoreceptors at PN22 (Fig. 6A). In early postnatal ages, some expression is in addition observed in the rod cell bodies in the outer nuclear layer (Fig. S4G). Rhodopsin positive cells were detected at 3DIV and 18DIV on both GaP NW and controls (Fig. 6B–C, Fig. S4H–I). At 3DIV, it was also possible to discern a mesh of rhodopsin labeled processes inside the clusters (not shown), and occasionally a process was seen extending outside a cluster (Fig. S4H–I). Processes emerging from single labeled cells were rare or very short and observed in cultures on both substrates. At 18DIV, however, rhodopsin expression was only observed in the cell soma.

The presence of cone photoreceptors in cultures was verified by immunostaining for cone arrestin. In PN7 normal mouse retinas, this protein was weakly expressed in cells scattered throughout the

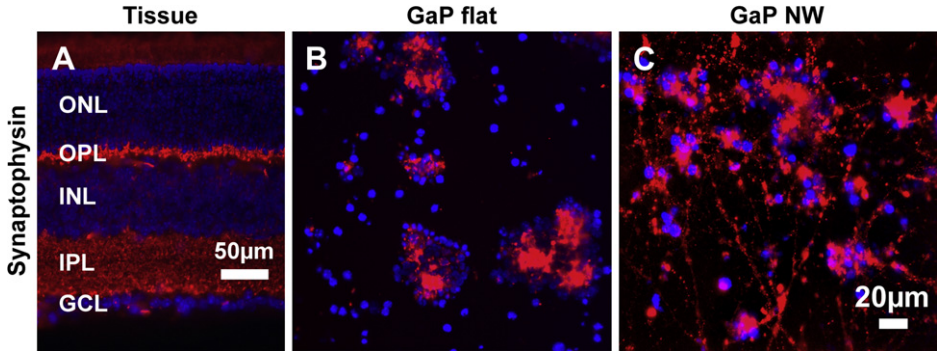

Fig. 5. Fluorescence images showing the distribution of synaptophysin (red) and cell nuclei (DAPI, blue) on (A) a retinal section at PN22, and in retinal cell cultures after 18DIV on (B) flat GaP and (C) GaP NW substrates. The NW were grown with a density of 1 NW/μm^2, a diameter of 80 nm and a length of 4 μm. ONL, outer nuclear layer; OPL, outer plexiform layer; INL, inner nuclear layer; IPL, inner plexiform layer; GCL, ganglion cell layer. Scale bar for retinal section, 50 μm. Scale bar for retinal cell cultures, 20 μm. (For interpretation of the references to color in this figure legend, the reader is referred to the web version of this article.)

outer and inner nuclear layers (not shown), whereas at PN22, distinct labeling was found in a subpopulation of cells in the outermost part of the outer nuclear layer, in their inner and outer segments and in terminals in the outer plexiform layer (Fig. 6D). Single cells and cluster cells expressing cone arrestin were found on both GaP NW and flat GaP at 3DIV and 18DIV (Fig. 6E–F). A few of these cells were also seen to extend short, labeled processes. Similarly to what was seen with rhodopsin, there seemed to be no significant difference in the number of cone arrestin positive cells between the two types of substrates.

We also tested an antibody against the calcium-binding protein, recoverin, which, *in vivo*, is expressed by photoreceptors and a subset of bipolar cells. At PN7, staining of variable intensity corresponding to recoverin was seen in cell bodies throughout the outer nuclear layer, in the short developing inner segments, and at the level of the outer plexiform layer (not shown). At PN22, weak cytoplasmatic staining was seen among photoreceptor cell bodies, whereas intense labeling was observed over the photoreceptor inner and outer segments, in the outer plexiform layer, and in a subpopulation of bipolar cells that projected labeled processes into the inner plexiform layer (Fig. 6G). A relatively large number of recoverin positive cells and labeled processes were observed in all cultures, irrespective of the substrate (Fig. 6H–I) or the duration of the culture, with no apparent differences between them.

Two other antibodies normally labeling bipolar cells were also used. Protein kinase C (PKC) was seen in normal retinas in cell bodies located in the outer part of the inner nuclear layer and in their processes projecting to the inner part of the inner plexiform layer (Fig. 7A). In all cultures, only a few PKC positive cells with no or very short processes were found in association with clusters (Fig. 7B–C). Chx10, a member of the *prd*-like class of homeodomain proteins, was expressed in sections in cell bodies in the inner nuclear layer both at PN7 and PN22, with the difference that at the younger age, labeled cells were located over most of the layer in the central retina (not shown), whereas at PN22 these were restricted mainly to the outer half (Fig. 7D). Chx10 labeled cells were found both at 3DIV and 18DIV in flat GaP and GaP NW (Fig. 7E–F), and as noted with PKC, with no discernable differences between the two substrates.

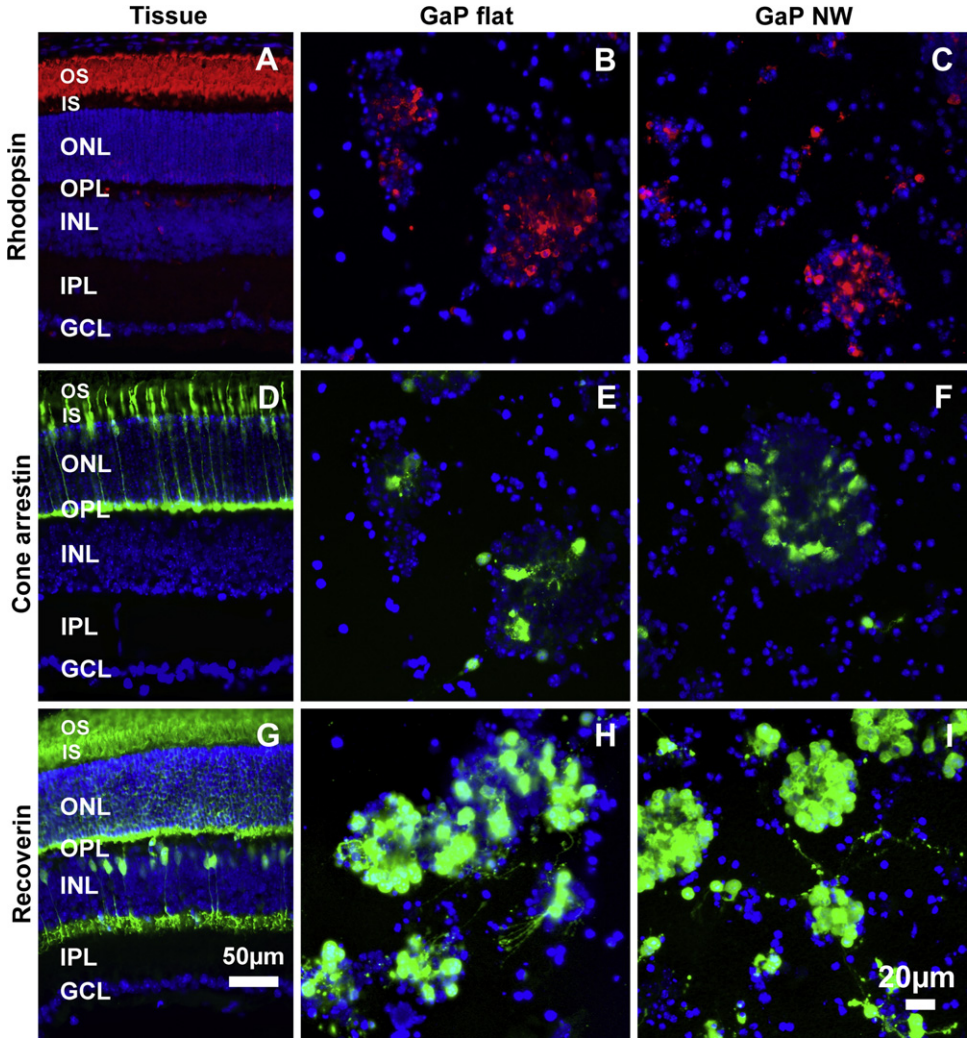

Fig. 6. Fluorescence images showing the distribution of: Rhodopsin (red) in (A) a retinal section at PN22, and in retinal cell cultures after 18DIV on (B) flat GaP and (C) GaP NW substrates; cone arrestin (green) in (D) a retinal section at PN22, and in retinal cell cultures after 18DIV on (E) flat GaP and (F) GaP NW substrates; recoverin (green) in (G) a retinal section at PN22, and in retinal cell cultures after 18DIV on (H) flat GaP and (I) GaP NW substrates. In all panels, cell nuclei were stained blue using DAPI. The NW were grown with a density of 1 NW/μm^2, a diameter of 80 nm and a length of 4 μm. OS, IS, photoreceptor inner and outer segments; ONL, outer nuclear layer; OPL; outer plexiform layer; INL, inner nuclear layer; IPL, inner plexiform layer; GCL, ganglion cell layer. Scale bar for retinal sections, 50 μm. Scale bar for retinal cell cultures, 20 μm. (For interpretation of the references to color in this figure legend, the reader is referred to the web version of this article.)

The presence of ganglion cells in the cultures was examined by immunostaining with antibodies localizing the POU-homeodomain factor Brn3a, and the transient receptor potential vanilloid 4 (TRPV4) channel. In normal mouse retinas, Brn3a was expressed in the nucleus of most cells located in the ganglion cell layer both at PN7 (Fig. S4J) and PN22 (Fig. 7G). TRPV4 labeling was restricted to the soma of cells in the ganglion cell layer and was in addition expressed in the nerve fiber layer (Fig. 7J). In cultures, Brn3a was observed in a number of cells associated with clusters at all time points examined and in both types of substrates. However, in contrast to the distribution seen in intact tissue, Brn3a appeared in all cultures to be expressed mainly in the perinuclear region. In addition, processes of various lengths and diameter were Brn3a positive (Fig. 7H–I, Fig. S4K–L). Already at 3DIV, the Brn3a labeled processes were longer and more abundant on GaP NW than on flat GaP (Fig. S4K–L). The difference between the two substrates

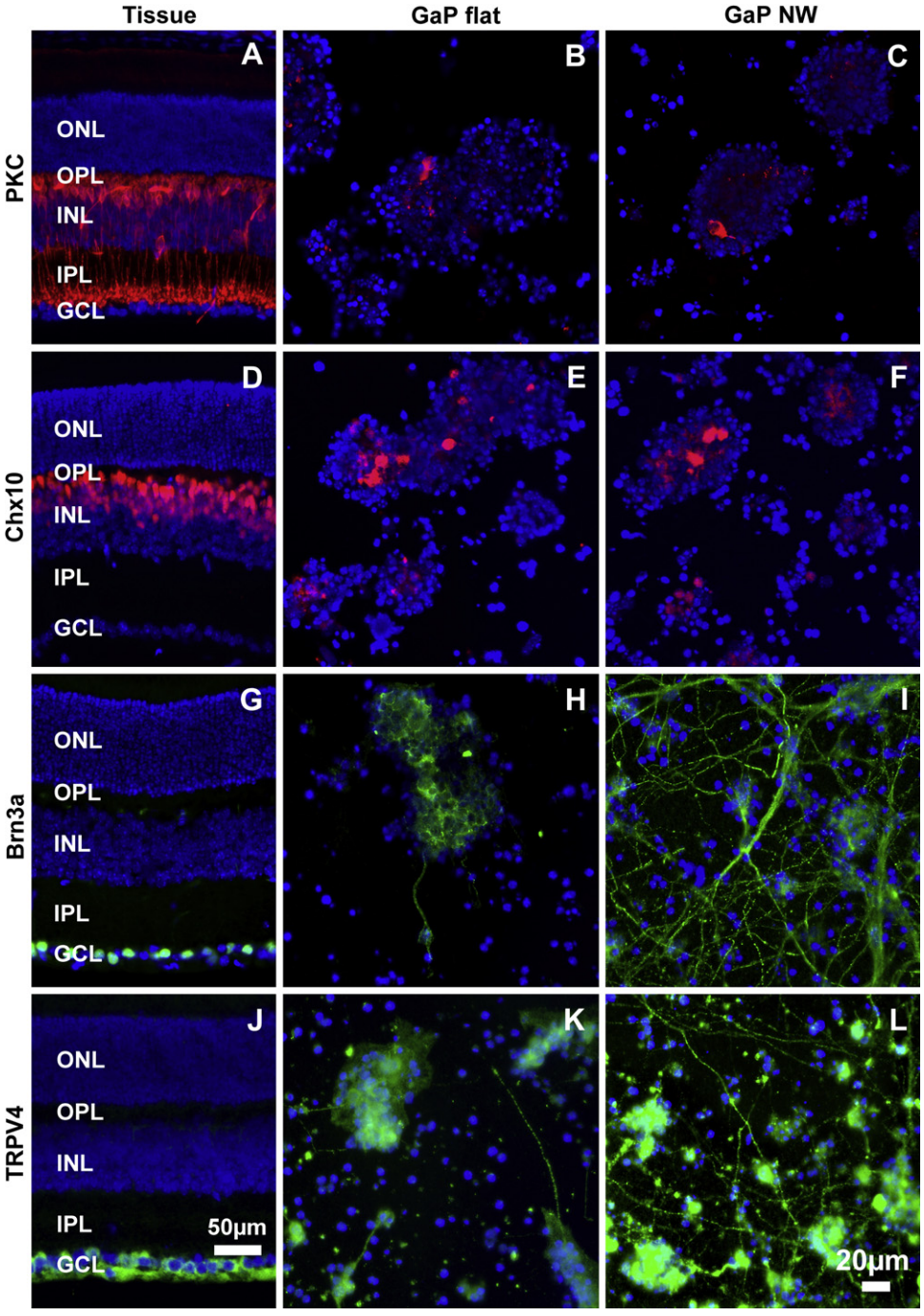

Fig. 7. Fluorescence images showing the distribution of: PKC (red) in (A) a retinal section at PN22, and in retinal cell cultures after 18DIV on (B) flat GaP and (C) GaP NW substrates; Chx10 (red) in (D) a retinal section at PN22, and in retinal cell cultures after 18DIV on (E) flat GaP and (F) GaP NW substrates; Brn3a (green) in (G) a retinal section at PN22, and in retinal cell cultures after 18DIV on (H) flat GaP and (I) GaP NW substrates; TRPV4 (green) in (J) a retinal section at PN22, and in retinal cell cultures after 18DIV on (K) flat GaP and (L) GaP NW substrates. In all panels, cell nuclei were stained blue using DAPI. The NW were grown with a density of 1 NW/μm^2, a diameter of 80 nm and a length of 4 μm. ONL, outer nuclear layer; OPL, outer plexiform layer; INL, inner nuclear layer; IPL, inner plexiform layer; GCL, ganglion cell layer. Scale bar for retinal sections, 50 μm. Scale bar for retinal cell cultures, 20 μm. (For interpretation of the references to color in this figure legend, the reader is referred to the web version of this article.)

became considerably more pronounced at 18DIV. On flat GaP, few Brn3a cells and processes were noted even in areas populated with nearby cell clusters, whereas a rich network of labeled processes was observed on GaP NW (Fig. 7H–I). Similar observations were made with TRPV4, which also labeled cell bodies and fibers in both substrates. Again, it was found that though the number of TRPV4 expressing processes in GaP NW was lower than seen for BRN3a, it was still higher than seen on flat GaP substrates (Fig. 7K–L). Since the *in vitro* conditions could potentially induce changes in protein expression, we performed also a colocalization analysis to further verify the identity of cells present in the GaP NW cultures. It was found that recoverin did not colocalize with β-tubulin III or with Chx10 (Fig. 8A–B). A few of the latter, however, colocalized with β-tubulin III (Fig. 8C) and with TRPV4 at 18DIV (Fig. 8D).

In PN4 mouse retinas, not only neurons but also glial cells are present. We therefore also stained the cultures for glial cell markers. Immunostaining with glial fibrillary acidic protein (GFAP) showed that at PN22, GFAP labeling is concentrated at the inner margin of the retina, corresponding to the location of astrocytes, and at the outer plexiform layer (Fig. 9A). In cultures, GFAP positive cells were detectable in both substrates at 3DIV and 18DIV, but the labeled cells exhibited distinct morphologies in the two. In flat GaP, most cells had a flat, polygonal appearance (Fig. 9B), whereas on GaP NW most cells possessed radial, slender processes emerging from the cell body (Fig. 9C). It was found also that the number of GFAP expressing cells tended to increase with time in culture with both substrates and that labeled cells often occurred in groups of adjacent cells, particularly on flat GaP substrates. Yet, a dominance of GFAP positive cells was never observed. The Müller glial cell marker, cellular retinaldehyde binding protein (CRALBP), was also used. In normal retinas, CRALBP was expressed in the retinal pigment epithelium and in the cell body and radial processes of the Müller glial cells; distinct labeling was also observed in the inner and outer limiting membranes (Fig. 9D). A few CRALBP expressing cells were detected at 3DIV (not shown) and their number was increased at 18DIV in both flat GaP and GaP NW, mainly in association with cell clusters (Fig. 9E–F), with no obvious differences between the two substrates. There was no indication that RPE cells were present in the cultures, therefore the CRALBP stained cells were likely to be Müller cells.

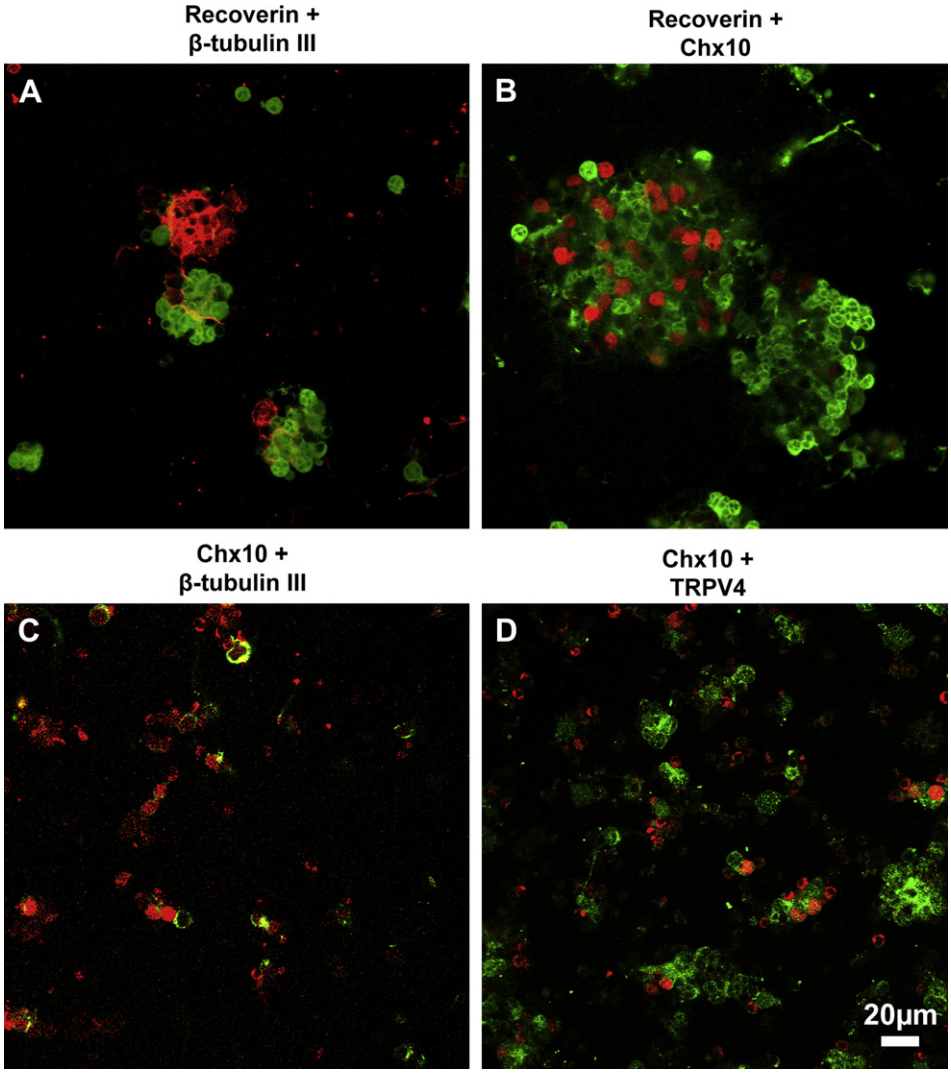

Fig. 8. Fluorescence images (optical slice 1 μm) showing retinal cells on GaP NW substrates after 18DIV colabeled with (A) recoverin (green) and β-tubulin III (red), (B) recoverin (green) and Chx10 (red), (C) Chx10 (red) and β-tubulin III (green) and (D) Chx10 (red) and TRPV4 (green). The NW were grown with a density of 1 NW/μm^2, a diameter of 80 nm and a length of 4 μm. In all images, the focus is on the cell bodies and not on the neuronal processes. Scale bar, 20 μm. (For interpretation of the references to color in this figure legend, the reader is referred to the web version of this article.)

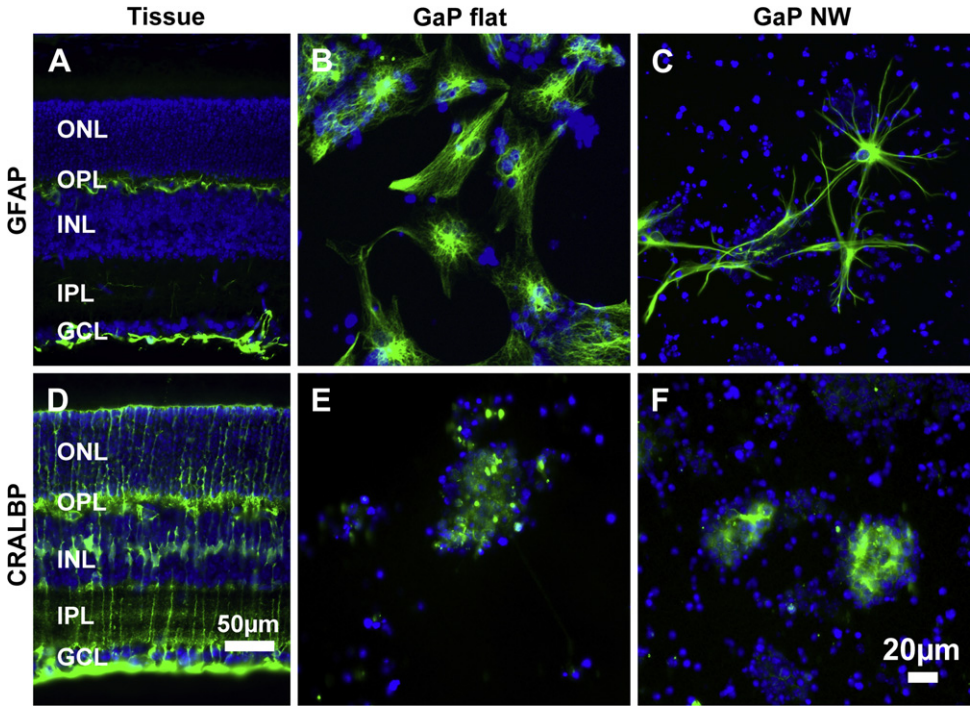

Fig. 9. Fluorescence images showing the distribution of GFAP (green) in (A) a retinal section at PN22, and in retinal cell cultures after 18DIV on (B) flat GaP and (C) GaP NW substrates; CRALBP (green) in (D) a retinal section at PN22, and in retinal cell cultures after 18DIV on (E) flat GaP and (F) GaP NW substrates. In all panels, cell nuclei were stained blue using DAPI. The NW were grown with a density of 1 NW/μm^2, a diameter of 80 nm and a length of 4 μm. ONL, outer nuclear layer; OPL, outer plexiform layer; INL, inner nuclear layer; IPL, inner plexiform layer; GCL, ganglion cell layer. Scale bar for retinal sections, 50 μm. Scale bar for retinal cell cultures, 20 μm. (For interpretation of the references to color in this figure legend, the reader is referred to the web version of this article.)

3.4. Effect of substrate HfO_x coating

In order to change the mechanical properties and the surface chemistry of the substrates, flat GaP and 40 nm diameter GaP NW were coated with a 20 nm thick HfO_x layer. This resulted in NW of the same diameter (80 nm) as used for the most part in the present study. As shown in Fig. S5, the HfO_x coating had no effect on the degree of neurite outgrowth on the flat substrates or on the NW substrates.

4. Discussion

Cell studies performed using semi-conductor NW substrates such as silicon, gallium phosphide or indium arsenide NW [1,8,12,13,18] have examined mostly non-neuronal cells (*e.g.,* HeLa cells, fibroblasts, epithelial and endothelial cell lines, mouse embryonic stem cells or human embryonic kidney cells) [13,18,34]. Cultures of neuronal cells on NW substrates have, to our knowledge, involved only a few cell types of the peripheral nervous system (PNS) [12,14], which were seen to survive for at least 3DIV.

The present study showed that central nervous system (CNS) cells derived from postnatal mouse retinas can survive on vertical GaP NW for at least 18DIV and that culturing on this substrate significantly enhances neurite outgrowth. Notably, our results contrast with those of a recent study showing that nanotube arrays of titanium dioxide (TiO_2) fail to support the survival of single retinal cells, while maintaining the viability and organization of retinal explants [35], an outcome which the authors attributed to an overall poor adhesion of the cells to the substrate. In our study, adhesion was observed on both substrates, flat GaP and GaP NW, but we found that the cell distribution was influenced by the NW.

4.1. Cell attachment and neurite extension

In GaP NW, numerous small cell clusters were found on the substrate while mostly big and medium size clusters and single cells were seen in flat substrates. It is not clear what caused this difference or when the difference was established. Despite passing the retinal cell suspensions through a 40 μm cell strainer and continuous dispersion, the dissociated cells tended to re-aggregate, resulting in a mixture of clusters of different sizes and single cells seeded on the substrates. However, in each trial, the cell suspension was seeded in a random order on both types of substrates, in order to avoid an uneven composition. Thus, the differences noted in cluster size between flat GaP and GaP NW are likely to have developed following seeding. Since the flat substrates are atomically flat and without any specific chemical coating for cell attachment, they are not optimal substrates for promoting cellular adhesion [14]. In these substrates, the cell–cell adhesion may therefore, at least initially, have been stronger than the cell–substrate adhesion, leading to the formation of bigger clusters. Adhesion on the flat substrate did occur, which may be mediated by impurities on the surface, but areas lacking cells were noticeable already at 3DIV and were larger at 18DIV, suggesting that there was an initial poorer attachment to the flat GaP surface and/or a greater detachment during the culture period or processing of the samples. The size of such areas varied considerably between different samples of flat GaP, precluding a meaningful quantification of the number of cells in these cultures. Thus, although no obvious differences in the number of dying and proliferating cells were noted between flat GaP and GaP NW, we might have an underestimation of their numbers in flat GaP because of a greater loss of cells. There was little evidence of cell detachment from GaP NW substrates over time, so the low number of dying cells found even at 18DIV would indicate that this substrate does support good long-term survival of retinal cells.

In the case of GaP NW, single cells and small clusters could simply become immobilized upon contact with the NW or they might actually adhere. In any case, it is conceivable that cells and clusters would have a limited mobility on the NW substrate compared to the flat surface, also contributing to a different cell distribution on the two topographies. Over time, cells are also likely to interact with the NW by more active mechanisms, *e.g.,* by forming focal adhesion contacts, as was previously found for cells derived from dorsal root ganglia [12,14,36], which would further contribute to a better attachment.

As shown here, NW influenced not only the cell distribution and attachment, but also the ability of the retinal cells to extend neurites in culture. It is well established that the surface topography influences neurite elongation and similar observations have been made for PNS neurons on GaP NW [12,14] and on functionalized carbon nanotubes [37]. We found, in addition, that of the topographical parameters tested, the length of the NW seemed to play a more crucial role in these processes, with the NW diameter and the density having little or no effect. Longer neuronal processes could be seen with 4 μm GaP NW already at 3DIV and the difference from flat GaP was even more pronounced at 18DIV.

It is not clear though by which mechanism(s) NW length determines the extent of neurite outgrowth. Both the surface chemistry and the mechanical properties of the NW could play a role. The NW intrinsic surface chemistry (*i.e.,* before exposure to any proteins present in the biological material, such as medium or cells) is determined by the crystalline structure, the exposed crystalline planes and the amount of dopants present in the crystal, which are different from those of the GaP wafer. Assuming these properties can influence neurite outgrowth, a bigger effect may be expected from longer NW. We therefore coated some NW substrates with an amorphous material (HfO_x) before the cell culture in order to ensure a uniform surface chemistry throughout the substrate [38]. However, since HfO_x is a stiffer material than GaP [39], this also changed the NW mechanical properties, which vary depending on the NW length, diameter and material. Cells are known to react differently depending on the substrate elasticity modulus [7,40,41]. We did not observe any significant changes in the distribution of cell clusters or in the degree of neurite extension when comparing the HfO_x coated NW to the GaP NW substrates, with the same topographical parameters.

In particular, in the case of HfO_x coating, the NW stiffness k can be approximated by Landau [42]:

$$k = 3EI/L^3 = 3E\pi\left(D_e^4 - D_i^4\right)\Big/\left(64L^3\right),$$

where E is the Young's modulus of the material, I is the second moment of inertia, L the nanowire length, D_e and D_i the external and internal diameters of the HfO_x shell, respectively. For a GaP NW of diameter D, the stiffness is:

$$k = 3EI/L^3 = 3E\pi D^4/\left(64L^3\right),$$

The Young's modulus of GaP is 160 MPa and the Young's modulus of HfO_x is 280 GPa [39]. Therefore coating 40 nm diameter GaP NW with HfO_x to a final diameter of 80 nm will increase the nanowire stiffness by a factor of 1600. As this increase in stiffness is equivalent to the effect of decreasing NW length to 500 nm, which we found had a negative effect on neurite extension, it may be concluded that the intrinsic surface chemistry and the mechanical properties of the substrate do not play a major role, or that these two effects compensate each other. Thus, it appears that the differences observed in neurite extension between short and long NW are most likely due to the length *per se* or to chemical modifications induced by the biological medium.

In a biological medium, the chemical and topographical properties of a substrate are strongly linked since protein deposition, adhesion, and conformation are affected by the micro-nanotopography of the substrate [34,43–46]. As shown for nanoparticles in biological fluids [44], the properties of the protein layer around a NW are likely to be specific to its topography and therefore might differ from those of a protein layer adsorbed on a flat surface. Therefore, on GaP NW substrates, the retinal cells could be subjected to protein concentration gradients, a situation that more closely resembles their native microenvironment, which would not be the case with flat substrates.

4.2. Retinal cell identification

Several protocols exist for the maintenance of primary retinal cells and cell lines in culture [47]. In the present study, a protocol used to culture retinal ganglion cells (RGC) was followed [31]. In the original study, adult rat retinas were used and cells were cultured for up to 7DIV on Poly-D-Lysine (PDL) and PDL/Laminin-coated culture plates. In these cultures, ganglion cells were the predominating cell type, whereas we were able to identify all the major retinal cell types in our cultures by using specific antibodies. The survival of different retinal cell types is generally greater when culturing young tissue, which could explain why not only ganglion cells thrived in the present study. Both in flat GaP and in GaP NW, mostly cells belonging to clusters were seen to express the markers tested. It was not possible to determine the number of cells expressing a given marker in each cluster, and a precise estimation of total cell number was also unreliable as cells and cell clusters detached from flat GaP substrates. However, there was no obvious indication that the survival of a particular retinal cell subtype was favored by any of the substrates.

The cell markers employed allowed us to identify rod and cone photoreceptors, bipolar cells as well as ganglion cells in the cultures, which appeared viable for as long as 18DIV in both substrates. However, differences were noted between the two. One of the most significant phenotypic effects of culturing the retinal cells on GaP NW was the extent of neurite outgrowth exhibited by a subpopulation of the cells. This was observed already at 3DIV and also at 18DIV with β-tubulin III, Brn3a and TRPV4, which all revealed the presence of a rich network of fibers interconnecting cell clusters in GaP NW substrates. β-tubulin III is a filamentous marker expressed mainly by inner retinal neurons [48] and found in our tissue samples in the inner plexiform and nerve fiber layers, which most likely corresponds to localization in dendrites and axons of RGC. We found no colocalization of β-tubulin III with recoverin (labels *photoreceptors and cone bipolar cells*) or Chx10 (which labels *bipolar cells and progenitor cells*), suggesting that the β-tubulin III positive cells and fibers found in GaP NW substrates are most likely RGCs. The presence of these cells in the cultures was further confirmed by localizing Brn3a, a POU-domain transcription factor found in a large subpopulation of RGCs [49]. The number of Brn3a expressing RGCs normally decreases during the first postnatal week *in vivo* and the cell loss is even more pronounced and prolonged *in vitro* as a result of the transection of the RGC axons [50]. Although quantification was not performed, there seemed to be no reduction over time in the number of Brn3a expressing cells in GaP NW substrates. Also notable is the fact that Brn3a was found not only in the cell nuclei, as was the case in the retinal sections, but also in the dense network of thin and thick processes reaching out of the cell clusters. The loss of cell–cell contact that occurs upon dissociation and the overall stress to which the cells are subjected in culture could certainly alter the levels and/or the pattern of distribution of a given protein, which might explain the prominent Brn3a expression in the neurites. However, this would

suggest that Brn3a can function not only as a transcriptional regulator, but may have also other functions. In culture, RGC processes lack their native cues, but are (under favorable conditions) still capable of extending. The GaP NW array provided a good substrate for neurite extension even without any coating, and it is possible that RGC utilize Brn3a in this process, along with other proteins. A few neurites were seen to extend for long distances over the GaP NW substrates, while the majority seemed to project to nearby cell clusters. In the present work, we showed that a number of these processes contained also synaptophysin, an integral membrane protein of small synaptic vesicles [51], indicating that the ability to form chemical synapses is preserved for at least 18DIV in cells grown on GaP NW substrates.

Another phenotypic effect of culturing the retinal cells on GaP NW was observed with glial cells, which exhibited clearly different morphologies on the two substrates. One possibility is that they corresponded to different types of cells. There are in the intact mouse retina two very distinct types of macroglial cells. Müller cells, located in the middle of the retina with long processes that extend over the whole retinal thickness and which do not express glial fibrillary acidic protein (GFAP), and astrocytes, which are located in the nerve fiber layer, in close association with the retinal ganglion cell axons and the vasculature, and express high constitutive levels of this filament [52]. On GaP NW substrates, the morphology of the GFAP labeled cells was similar to that of astrocytes in intact retinas, which would suggest that this glial cell type had an advantage over Müller cells in the presence of NW. However, despite the differences noted *in vivo*, the two cell types are not easily distinguished *in vitro*, since in culture they exhibit atypical morphologies and can both express GFAP. Moreover, cells expressing cellular retinaldehyde binding protein (CRALBP), which is found *in vivo* in Müller cells but not astrocytes, were also observed on both substrates. Another possibility is that the NW affected the degree of maturation of the glial cells with resulting changes in their morphology, as previously shown for brain astrocytes cultured in the presence of carbon nanotubes [53]. Staining for Ki-67 revealed the presence of a few dividing cells on both substrates at 3DIV and 18DIV, most of which were likely to be glial cells. However, as many cells detached from flat GaP, the number of dividing cells on this substrate was probably in fact larger, which would explain why large areas of cell confluence were observed. It is thus possible that glial cells on flat GaP were kept in a less differentiated, more proliferative state than those on GaP NW. Although further assessment of how retinal glial cells interact with GaP NW is necessary, our results seem to be consistent with those of previous studies showing that there is a decreased adhesion of astrocytes to nanostructured surfaces than to smooth surfaces These observations are validated also by *in vivo* studies, which showed a lower tissue response to nanostructured surfaces [3,11] These findings are of significance, as extensive glial proliferation would contribute to form a larger glial scar around an implantable device, limiting its long-term performance.

5. Conclusions

We report that epitaxial GaP NW substrates support the long-term survival of multiple retinal cell types and the elongation of neuronal processes. We showed that neurite outgrowth was greatest with the longest NW (4 μm) and that intrinsic NW-surface chemistry and NW mechanical properties are not likely to play a significant role in this process. We speculate that protein concentration gradients in the protein corona around the NW and/or the length *per se*, which affects the NW spatial configuration, are important factors in promoting neurite outgrowth on NW substrates. Our study also showed that glial cells in GaP NW did not overgrow neurons even after 18DIV. The observation that GaP NW substrates with a specific topography enable the sprouting of CNS neurons without favoring the spreading/adhesion of glial cells provides new input regarding the potential use of GaP NW in biological systems. The fact that the topographical features of GaP NW can be fully controlled, together with the data reported here, warrants further investigations of the *in vivo* biocompatibility of GaP NW (and of equivalent materials) as these could be incorporated in, for instance, retinal implants.

Acknowledgments

The authors would like to thank Drs. Robert S Molday, Cheryl Craft and John C Saari for the generous gift of antibodies, Hodan Abdshill for assistance with retinal dissection and preparation of media, Birgitta Klefbohm for maintaining the animal colony and Henrik Persson for growing the nanowires. Gaëlle Piret was financed by a postdoctoral grant from the Lund Tekniska Högskola (LTH) at Lund University. The study was supported by the Nanometer Structure Consortium (nmC@LU), the Swedish Research Council, Ögonfonden, VELUX STIFTUNG, Edwin Jordans Stiftelse för Oftalmologisk Forskning, Gun och Bertil Stohnes Stiftelse, Greta och Johan Kocks Stiftelse, Magnus Bergvalls Stiftelse, and the Neuronano Research Center at Lund University.

Appendix A. Supplementary data

Supplementary data related to this article can be found at http://dx.doi.org/10.1016/j.biomaterials.2012.10.042.

References

[1] Martínez E, Engel E, Planell JA, Samitier J. Effects of artificial micro- and nano-structured surfaces on cell behaviour. Ann Anat 2009;191:126–35.
[2] McMurray RJ, Gadegaard N, Tsimbouri PM, Burgess KV, McNamara LE, Tare R, et al. Nanoscale surfaces for the long-term maintenance of mesenchymal stem cell phenotype and multipotency. Nat Mater 2011;10:637–44.
[3] Moxon KA, Kalkhoran NM, Markert M, Sambito MA, McKenzie JL, Webster JT. Nanostructured surface modification of ceramic-based microelectrodes to enhance biocompatibility for a direct brain-machine interface. IEEE Trans Biomed Eng 2004;51:881–9.
[4] Liu H, Webster TJ. Nanomedicine for implants: a review of studies and necessary experimental tools. Biomaterials 2007;28:354–69.
[5] Kotov NA, Winter JO, Clements IP, Jan E, Timko BP, Campidelli S, et al. Nanomaterials for neural interfaces. Adv Mater 2009;21:3970–4004.
[6] Gelain F, Panseri S, Antonini S, Cunha C, Donega M, Lowery J, et al. Transplantation of nanostructured composite scaffolds results in the regeneration of chronically injured spinal cords. ACS Nano 2010;5:227–36.
[7] Teo BKK, Ankam S, Chan LY, Yim EKF. Nanotopography/mechanical induction of stem-cell differentiation. In: Shivashankar GV, editor. Methods in cell biology. Academic Press; 2010. p. 241–94.
[8] Shalek AK, Robinson JT, Karp ES, Lee JS, Ahn D-R, Yoon M-H, et al. Vertical silicon nanowires as a universal platform for delivering biomolecules into living cells. Proc Natl Acad Sci U S A 2010;107:1870–5.
[9] Donoghue JP. Connecting cortex to machines: recent advances in brain interfaces. Nat Neurosci 2002;5:1085–8.
[10] Schouenborg J. Biocompatible multichannel electrodes for long-term neurophysiological studies and clinical therapy-novel concepts and design. Prog Brain Res 2011;194:61–70.
[11] Keefer EW, Botterman BR, Romero MI, Rossi AF, Gross GW. Carbon nanotube coating improves neuronal recordings. Nat Nanotechnol 2008;3:434–9.
[12] Hallstrom W, Martensson T, Prinz C, Gustavsson P, Montelius L, Samuelson L, et al. Gallium phosphide nanowires as a substrate for cultured neurons. Nano Lett 2007;7:2960–5.
[13] Kim W, Ng JK, Kunitake ME, Conklin BR, Yang PD. Interfacing silicon nanowires with mammalian cells. J Am Chem Soc 2007;129:7228–9.
[14] Prinz C, Hallstrom W, Martensson T, Samuelson L, Montelius L, Kanje M. Axonal guidance on patterned free-standing nanowire surfaces. Nanotechnology 2008;19:345101.
[15] Hallstrom W, Prinz CN, Suyatin D, Samuelson L, Montelius L, Kanje M. Rectifying and sorting of regenerating axons by free-standing nanowire patterns: a highway for nerve fibers. Langmuir 2009;25:4343–6.
[16] Linsmeier CE, Prinz CN, Pettersson LME, Caroff P, Samuelson L, Schouenborg J, et al. Nanowire biocompatibility in the brain – looking for a needle in a 3d stack. Nano Lett 2009;9:4184–90.

[17] Hallstrom W, Lexholm M, Suyatin DB, Hammarin G, Hessman D, Samuelson L, et al. Fifteen-piconewton force detection from neural growth cones using nanowire arrays. Nano Lett 2010;10:782–7.
[18] Berthing T, Bonde S, Sorensen CB, Utko P, Nygard J, Martinez KL. Intact mammalian cell function on semiconductor nanowire arrays: new perspectives for cell-based biosensing. Small 2011;7:640–7.
[19] Safi M, Yan M, Guedeau-Boudeville M-A, Conjeaud Hln, Garnier-Thibaud V, Boggetto N, et al. Interactions between magnetic nanowires and living cells: uptake, toxicity, and degradation. ACS Nano 2011;5:5354–64.
[20] Bucaro MA, Vasquez Y, Hatton BD, Aizenberg J. Fine-tuning the degree of stem cell polarization and alignment on ordered arrays of high-aspect-ratio nanopillars. ACS Nano 2012;6:6222–30.
[21] Seifert W, Borgstrom M, Deppert K, Dick KA, Johansson J, Larsson MW, et al. Growth of one-dimensional nanostructures in MOVPE. J Cryst Growth 2004; 272:211–20.
[22] Suyatin DB, Hallstram W, Samuelson L, Montelius L, Prinz CN, Kanje M. Gallium phosphide nanowire arrays and their possible application in cellular force investigations. J Vac Sci Technol B 2009;27:3092–4.
[23] Zhang Y, Arnér K, Ehinger B, Perez MT. Limitation of anatomical integration between subretinal transplants and the host retina. Invest Ophthalmol Vis Sci 2003;44:324–31.
[24] Grüter O, Kostic C, Crippa SV, Perez MT, Zografos L, Schorderet DF, et al. Lentiviral vector-mediated gene transfer in adult mouse photoreceptors is impaired by the presence of a physical barrier. Gene Ther 2005;12:942–7.
[25] Singhal S, Lawrence JM, Bhatia B, Ellis JS, Kwan AS, MacNeil A, et al. Chondroitin sulfate proteoglycans and microglia prevent migration and integration of grafted Müller stem cells into degenerating retina. Stem Cells 2008;26: 1074–82.
[26] Zarbin MA, Montemagno C, Leary JF, Ritch R. Nanotechnology in ophthalmology. Can J Ophthalmol 2010;45:457–76.
[27] Redenti S, Tao S, Yang J, Gu P, Klassen H, Saigal S, et al. Retinal tissue engineering using mouse retinal progenitor cells and a novel biodegradable, thin-film poly(e-caprolactone) nanowire scaffold. J Ocul Biol Dis Infor 2008;1:19–29.
[28] Chader GJ, Weiland J, Humayun MS. Artificial vision: needs, functioning, and testing of a retinal electronic prosthesis. Prog Brain Res 2009;175:317–32.
[29] Matthaei M, Zeitz O, Keseru M, Wagenfeld L, Hornig R, Post N, et al. Progress in the development of vision prostheses. Ophthalmologica 2011;225:187–92.
[30] Magnusson MH, Deppert K, Malm J-O, Bovin J-O, Samuelson L. Size-selected gold nanoparticles by aerosol technology. Nanostruct Mater 1999;12:45–8.
[31] Grozdanov V, Müller A, Sengottuvel V, Leibinger M, Fischer DA. Method for preparing primary retinal cell cultures for evaluating the neuroprotective and neuritogenic effect of factors on axotomized mature CNS neurons. Curr Protoc Neurosci 2010;53:3.22.1–3.22.10.
[32] Caffé AR, Ahuja P, Holmqvist B, Azadi S, Forsell J, Holmqvist I, et al. Mouse retina explants after long-term culture in serum free medium. J Chem Neuroanat 2002;22:263–73.
[33] Wunderlich KA, Leveillard T, Penkowa M, Zrenner E, Perez MT. Altered expression of metallothionein-I and -II and their receptor megalin in inherited photoreceptor degeneration. Invest Ophthalmol Vis Sci 2010;51:4809–20.
[34] Piret G, Galopin E, Coffinier Y, Boukherroub R, Legrand D, Slomianny C. Culture of mammalian cells on patterned superhydrophilic/superhydrophobic silicon nanowire arrays. Soft Matter 2011;7:8642–9.
[35] Dallacasagrande V, Zink M, Huth S, Jakob A, Müller M, Reichenbach A, et al. Tailoring substrates for long-term organotypic culture of adult neuronal tissue. Adv Mater 2012;24:2399–403.
[36] Malmström J, Christensen B, Jakobsen HP, Lovmand J, Foldbjerg R, Sørensen ES, et al. Large area protein patterning reveals nanoscale control of focal adhesion development. Nano Lett 2010;10:686–94.
[37] Matsumoto K, Sato C, Naka Y, Whitby R, Shimizu N. Stimulation of neuronal neurite outgrowth using functionalized carbon nanotubes. Nanotechnology 2010;21:115101.
[38] Henrich VE, Cox PA. The surface science of metal oxides. New York: Cambrige University Press;; 1994.
[39] Dole SL, Hunter O, Wooge CJ. Elastic properties of monoclinic hafnium oxide at room temperature. J Am Ceram Soc 1977;60:488–90.
[40] Discher DE, Janmey P, Wang Y-l. Tissue cells feel and respond to the stiffness of their substrate. Science 2005;310:1139–43.
[41] Tee S-Y, Fu J, Chen Christopher S, Janmey Paul A. Cell shape and substrate rigidity both regulate cell stiffness. Biophys J 2011;100:25–7.
[42] Landau ED, Lifshizt EM. Theory of elasticity. Pergamon Press; 1959.
[43] Roach P, Farrar D, Perry CC. Surface tailoring for controlled protein adsorption: effect of topography at the nanometer scale and chemistry. J Am Chem Soc 2006;128:3939–45.
[44] Cedervall T, Lynch I, Lindman S, Berggard T, Thulin E, Nilsson H, et al. Understanding the nanoparticle-protein corona using methods to quantify exchange rates and affinities of proteins for nanoparticles. Proc Natl Acad Sci U S A 2007;104:2050–5.
[45] Koc Y, de Mello AJ, McHale G, Newton MI, Roach P, Shirtcliffe NJ. Nano-scale superhydrophobicity: suppression of protein adsorption and promotion of flow-induced detachment. Lab Chip 2008;8:582–6.
[46] Bhushan B, Jung YC. Natural and biomimetic artificial surfaces for superhydrophobicity, self-cleaning, low adhesion, and drag reduction. Prog Mater Sci 2011;56:1–108.
[47] Seigel GM. The golden age of retinal cell culture. Mol Vis 1999;5:4.
[48] Geller SF, Guerin KI, Visel M, Pham A, Lee ES, Dror AA, et al. CLRN1 is nonessential in the mouse retina but is required for cochlear hair cell development. PLoS Genet 2009;5:e1000607.
[49] Quina LA, Pak W, Lanier J, Banwait P, Gratwick K, Liu Y, et al. Brn3a-expressing retinal ganglion cells project specifically to thalamocortical and collicular visual pathways. J Neurosci 2005;25:11595–604.
[50] Voyatzis S, Muzerelle A, Gaspar P, Nicol X. Modeling activity and target-dependent developmental cell death of mouse retinal ganglion cells ex vivo. PLoS One 2012;7:e31105.
[51] Wiedenmann B, Franke WW. Identification and localization of synaptophysin, an integral membrane glycoprotein of Mr 38,000 characteristic of presynaptic vesicles. Cell 1985;41:1017–28.
[52] Sarthy PV, Fu M, Huang J. Developmental expression of the glial fibrillary acidic protein (GFAP) gene in the mouse retina. Cell Mol Neurobiol 1991;11: 623–37.
[53] Gottipati MK, Kalinina I, Bekyarova E, Haddon RC, Parpura V. Chemically functionalized water-soluble single-walled carbon nanotubes modulate morpho-functional characteristics of astrocytes. Nano Lett 2012;12: 4742–7.
[54] Geller SF, Lewis GP, Anderson DH, Fisher SK. Use of the MIB-1 antibody for detecting proliferating cells in the retina. Invest Ophthalmol Vis Sci 1995;36: 737–44.
[55] Hicks D, Molday RS. Differential immunogold-dextran labeling of bovine and frog rod and cone cells using monoclonal antibodies against bovine rhodopsin. Exp Eye Res 1986;42:55–71.
[56] Zhu X, Li A, Brown B, Weiss ER, Osawa S, Craft CM. Mouse cone arrestin expression pattern: light induced translocation in cone photoreceptors. Mol Vis 2002;8:462–71.
[57] Milam AH, Dacey DM, Dizhoor AM. Recoverin immunoreactivity in mammalian cone bipolar cells. Vis Neurosci 1993;10:1–12.
[58] Ruether K, Feigenspan A, Pirngruber J, Leitges M, Baehr W, Strauss O. PKCα is essential for the proper activation and termination of rod bipolar cell response. Invest Ophthalmol Vis Sci 2010;51:6051–8.
[59] Liu ISC, J-d Chen, Ploder L, Vidgen D, van der Kooy D, Kalnins VI, et al. Developmental expression of a novel murine homeobox gene (Chx10): evidence for roles in determination of the neuroretina and inner nuclear layer. Neuron 1994;13:377–93.
[60] Ryskamp DA, Witkovsky P, Barabas P, Huang W, Koehler C, Akimov NP, et al. The polymodal ion channel transient receptor potential vanilloid 4 modulates calcium flux, spiking rate, and apoptosis of mouse retinal ganglion cells. J Neurosci 2011;31:7089–101.
[61] Bunt-Milam AH, Saari JC. Immunocytochemical localization of two retinoid-binding proteins in vertebrate retina. J Cell Biol 1983;97:703–12.